A FRET biosensor, SMART, monitors necroptosis in renal tubular epithelial cells in a cisplatin-induced kidney injury model

Shin Murai[1], Kanako Takakura[2], Kenta Sumiyama[3], Kenta Moriwaki[1], Kenta Terai[4], Sachiko Komazawa-Sakon[1], Yoshifumi Yamaguchi[5], Tetuo Mikami[6], Kimi Araki[7,8], Masaki Ohmuraya[9], Michiyuki Matsuda[4, 10, 11], Hiroyasu Nakano[1]*

[1]Department of Biochemistry, Toho University School of Medicine, 5-21-16 Omori-Nishi, Ota-ku, Tokyo 143-8540, Japan.

[2]Imaging Platform for Spatio-Temporal Regulation, Graduate School of Medicine, Kyoto University, Kyoto 606-8501, Japan.

[3]Laboratory for Mouse Genetic Engineering, RIKEN Center for Biosystems Dynamics Research, Suita 565-0874, Japan.

[4]Research Center for Dynamic Living Systems, Graduate School of Biostudies, Kyoto University, Kyoto 606-8501, Japan.

[5]Hibernation metabolism, physiology, and development Group, Environmental Biology Division, Institute of Low Temperature Science, Hokkaido University, Kita 19, Nishi 8, Kita-ku, Sapporo, Hokkaido 060-0819, Japan

[6]Department of Pathology, Toho University School of Medicine, 5-21-16 Omori-Nishi, Ota-ku, Tokyo 143-8540, Japan.

[7]Center for Animal Resources and Development, Kumamoto University, 2–2–1 Honjo, Chuo-ku, Kumamoto 860-0811, Japan.

[8]Center for Metabolic Regulation of Healthy Aging, Kumamoto University, 1-1-1, Honjo, Chuo-ku, Kumamoto 860-8556, Japan.

[9]Department of Genetics, Hyogo College of Medicine, Nishinomiya, Hyogo 663-8501, Japan.

[10]Department of Pathology and Biology of Diseases, Graduate School of Medicine, Kyoto University, Kyoto 606-8501, Japan.

[11]Institute for Integrated Cell-Material Sciences, Kyoto University, Kyoto 606-8501, Japan.

*To whom correspondence should be addressed. E-mail: hiroyasu.nakano@med.toho-u.ac.jp

Abstract

Necroptosis is a regulated form of cell death involved in various pathological conditions, including ischemic reperfusion injuries, virus infections, and drug-induced tissue injuries. However, it is not fully understood when and where necroptosis occurs *in vivo*. We previously generated a Forster resonance energy transfer (FRET) biosensor, termed SMART (the sensor for MLKL activation based on FRET), which specifically monitored necroptosis in human and murine cell lines *in vitro*. Here, we generated transgenic (Tg) mice that expressed the SMART biosensor in various tissues. SMART monitored necroptosis, but not apoptosis or pyroptosis, in primary cells, including peritoneal macrophages and embryonic fibroblasts. Moreover, the FRET signal was elevated in renal tubular cells of cisplatin-treated SMART Tg mice compared to untreated SMART Tg mice. Together, SMART Tg mice may provide a valuable tool for monitoring necroptosis in different types of cells *in vitro* and *in vivo*.

50 **Introduction**

51 Necroptosis is a regulated form of cell death characterized by necrotic morphology.
52 Necroptosis is involved in various pathological conditions, including tumor necrosis
53 factor (TNF)-mediated systemic inflammatory response syndrome (SIRS), ischemic
54 reperfusion injury, neurodegeneration, and drug-induced tissue injuries [1, 2]. Necroptosis
55 is induced by death ligands (e.g., TNF, Fas ligand, and TRAIL), polyinosinic-
56 polycytidylic acid, lipopolysaccharide (LPS), interferon (IFN)α/β, IFNγ, some virus
57 infections, and endogenous Z-form nucleic acids [3, 4, 5]. Among the various signaling
58 pathways that lead to necroptosis, the TNF-mediated signaling pathway is one of the most
59 extensively investigated [6, 7]. In most cell types, TNF induces cell survival and
60 inflammatory cytokine expression by activating the transcription factor, nuclear factor
61 kappa B (NF-κB). However, under certain conditions, NF-κB activation is compromised,
62 for example, when transforming growth factor β (TGFβ)-activated kinase 1 (TAK1) or
63 inhibitor of apoptosis proteins (IAPs) are inhibited. Under those conditions, TNF induces
64 apoptosis or necroptosis in a context-dependent manner [6, 7]. Of note, under normal
65 conditions, caspase 8 suppresses necroptosis by cleaving and inactivating receptor-
66 interacting kinase 1 (RIPK1), an essential component of the TNF-induced necroptosis
67 pathway [8, 9]. When caspase 8 activity is blocked, either chemically, genetically, or by viral

68 infection, RIPK1 recruits RIPK3 via a homotypic interaction to form a necroptosis-
69 inducing signaling complex, termed the necrosome [10, 11, 12]. In necrosomes, RIPK3 is
70 activated by autophosphorylation, which leads to the formation of a higher-order
71 amyloid-like RIPK1-RIPK3 hetero-oligomer [13, 14]. Activated RIPK3 interacts with and
72 phosphorylates the mixed lineage kinase domain-like pseudokinase (MLKL) [15].
73 Phosphorylated MLKL forms a homo-oligomer and translocates to the cell membrane to
74 execute necroptosis [16, 17, 18, 19]

75 The ruptured membranes of dying cells release intracellular contents, which are
76 referred to as damage-associated molecular patterns (DAMPs). DAMPs comprise various
77 molecules, including heat shock proteins (HSPs), high mobility group protein B1
78 (HMGB1), ATP, and histones. Thus, DAMPs have pleiotropic functions that become
79 active in a context-dependent manner [20, 21]. However, it remains unclear when and where
80 cells undergo necroptosis and release DAMPs. We previously developed a Forster
81 resonance energy transfer (FRET) biosensor that could specifically monitor necroptosis,
82 which we termed the sensor for MLKL activation based on FRET (SMART) [22]. To
83 visualize the release of DAMPs at single-cell resolution, we modified a new technology
84 termed Live Cell Imaging for Secretion activity (LCI-S). This technology comprises a
85 fluorescence-conjugated, antibody-based sandwich ELISA system and total inverted

86 reflection fluorescence microscopy [23, 24]. By combining the SMART and LCI-S
87 technologies, we could visualize the execution of necroptosis and the release of HMGB1
88 (a nuclear DAMP) at single-cell resolution [22].

89 Here, we aimed to apply the SMART biosensor to *in vivo* experiments. We
90 generated transgenic (Tg) mice that stably expressed SMART in various tissues. SMART
91 Tg mice grew to adulthood without any apparent abnormality and were fertile. Consistent
92 with previous results in tumor cell lines that expressed SMART, the FRET to cyan
93 fluorescent protein (FRET/CFP) ratio was increased in peritoneal macrophages and
94 murine embryonic fibroblasts (MEFs) from SMART Tg mice along with progression of
95 necroptosis, but not apoptosis or pyroptosis. These results suggested that SMART
96 specifically monitored necroptosis in primary cells. Furthermore, in a cisplatin-induced
97 kidney injury model, the FRET/CFP ratio of renal proximal tubule cells increased in
98 SMART Tg mice compared to untreated SMART Tg mice. Collectively, we conclude that
99 SMART Tg mice may be a valuable tool for monitoring necroptosis *in vivo*.

100

101 ## Results

102 **Generation of SMART Tg mice.** The SMART is an intramolecular FRET biosensor. It
103 comprises a fragment of the kinase-like domain of MLKL, placed between the enhanced
104 cyan fluorescent protein (ECFP) sequence and the modified yellow fluorescent protein
105 (Ypet) sequence. The fluorescent proteins serve as the FRET donor and acceptor,
106 respectively (Fig. 1a, *upper panel*) [22, 25]. In the presence of stimuli that induce
107 necroptosis, RIPK3 is phosphorylated and subsequently oligomerizes, eliciting a
108 conformational change in SMART. This conformational change increases the FRET
109 efficiency, and the fluorescent signal changes from ECFP to Ypet (Fig. 1a, *lower panel*).

110 To visualize necroptosis under various pathological conditions *in vivo*, we used
111 the transposon system to generate transgenic mice that expressed SMART under the CAG
112 promoter, as described previously [26]. SMART Tg mice grew without any apparent
113 abnormality, and they were fertile. These mice stably expressed SMART in various
114 tissues, including the liver, spleen, kidney, small intestine, and colon (Fig. 1b). To test
115 whether SMART could monitor necroptosis in primary cells, as previously demonstrated
116 in tumor cell lines [22], we isolated peritoneal macrophages from SMART Tg mice. Briefly,
117 we performed an intraperitoneal injection of thioglycollate in mice to recruit
118 inflammatory macrophages into the peritoneal cavity; then, 4 days later, we collected the

119 macrophages. Approximately 80% of the collected peritoneal cells expressed both CD11b
120 and F4/80; therefore, these cells were considered macrophages (Fig. 1c, *left panel*). In
121 addition, the expression of yellow fluorescent protein (YFP) confirmed that these
122 macrophages expressed SMART (Fig. 1c, *right panel*).

123 When macrophages are treated with the IAP inhibitor, BV6, macrophages
124 produce TNF that can result in TNF-dependent apoptosis or necroptosis in a context-
125 dependent manner [27, 28]. In the presence of the caspase inhibitor, zVAD, BV6 treatment
126 induces necroptosis. When we stimulated macrophages with BV6/zVAD, the release of
127 lactate dehydrogenase (LDH), a hallmark of membrane rupture, gradually increased.
128 However, this increase was completely abolished when cells were treated with
129 BV6/zVAD in the presence of the RIPK3 inhibitor, GSK'872 (Fig. 1d). Live cell imaging
130 revealed that the FRET/CFP ratio gradually increased in cells treated with BV6/zVAD,
131 and then it abruptly declined (Fig. 1e, f, Supplementary movie 1). The FRET/CFP ratio
132 decline could have been due to the release of the SMART biosensor through the ruptured
133 membrane. In contrast, the FRET/CFP did not increase in untreated cells or cells treated
134 with BV6/zVAD/GSK'872 (Fig. 1e, f).

135

136 **SMART does not monitor pyroptosis or apoptosis.** We previously reported that

137 SMART could monitor necroptosis, but not apoptosis, in various human and murine cell
138 lines [22]. However, it remained unclear whether SMART could monitor pyroptosis. To
139 address this issue, we pretreated peritoneal macrophages from SMART Tg mice with LPS,
140 followed by nigericin stimulation. LPS plus nigericin, but not LPS alone, caused a robust
141 release of LDH from macrophages (Fig. 2a), which suggested that the macrophages died
142 by pyroptosis. The FRET/CFP ratio did not increase; instead, it eventually decreased in
143 cells treated with LPS/nigericin compared to cells treated with LPS alone (Fig. 2b, c,
144 Supplementary movie 2).

145 Priming macrophages with LPS and subsequently stimulating them with the
146 TAK1 inhibitor, 5z-7-oxozeaneaeol (5z7Ox), can result in apoptosis, necroptosis, or
147 pyroptosis, depending on the context [29, 30, 31]. To induce necroptosis selectively, we
148 primed macrophages with LPS, then stimulated them with 5z7Ox in the presence of
149 zVAD. In parallel experiments, after priming, we stimulated macrophages with 5z7Ox
150 in the presence of GSK'872 to induce apoptosis or pyroptosis. Macrophage viability
151 decreased under both of the latter conditions, but viability was maintained when cells
152 were stimulated with LPS/5z7Ox/GSK'872/zVAD, which blocked apoptosis,
153 necroptosis, and pyroptosis (Fig. 2d). Of note, the FRET/CFP ratio increased in cells
154 stimulated with LPS/5z7Ox/zVAD (necroptotic condition), but not in cells treated with

155 LPS/5z7Ox/GSK'872 (apoptotic or pyroptotic condition) (Fig. 2e, f). These results
156 suggested that SMART could monitor necroptosis, but not apoptosis or pyroptosis, in
157 primary macrophages.
158
159 **SMART monitors necroptosis in a RIPK3-dependent manner.** Necroptosis depends
160 on the activities of RIPK3 and MLKL [3, 32]. To further substantiate our finding, we tested
161 whether SMART could monitor RIPK3-dependent necroptosis in primary macrophages,
162 as observed in tumor cell lines [22]. To that end, we generated SMART Tg mice with a
163 *Ripk3-/-* genetic background (SMART *Ripk3-/-* mice). We prepared peritoneal
164 macrophages from SMART *Ripk3-/-* mice. In contrast to macrophages from SMART
165 WT mice, BV6/zVAD-induced LDH release was abrogated in macrophages from
166 SMART *Ripk3-/-* mice (Fig. 3a). Accordingly, the increase in the FRET/CFP ratio was
167 abolished in macrophages from SMART *Ripk3-/-* mice after BV6/zVAD stimulation
168 compared to those from SMART WT mice (Fig. 3b, c). These results showed that
169 increased FRET/CFP ratio in primary macrophages depended on RIPK3.
170
171 **SMART monitors necroptosis, but not apoptosis, in MEFs.** To extend our
172 observations in peritoneal macrophages to other cell types, we next stimulated primary

173 MEFs derived from SMART Tg mice. We found that TNF/BV6/zVAD stimulation did
174 not cause cell death in primary MEFs (pMEFs), but did cause cell death in immortalized
175 MEFs (iMEFs) (Fig. 4a, b). We noticed that MLKL expression was much lower in
176 pMEFs than in iMEFs (Fig. 4c). Because MLKL expression is induced by interferons [33,
177 34], we treated pMEFs with IFNβ. MLKL expression was strongly enhanced;
178 accordingly, IFNβ-pretreated pMEFs died in response to TNF/BV6/zVAD stimulation
179 (Fig. 4d). In addition, the FRET/CFP ratio was increased in IFNβ-pretreated pMEFs
180 after TNF/BV6/zVAD stimulation, but this increase was abolished in the presence of
181 GSK'872 (Fig. 4e, f, Supplementary movie 3). Moreover, when IFNβ-pretreated
182 pMEFs were stimulated with TNF/BV6/GSK'872, apoptosis was induced, but the
183 FRET/CFP ratio was not increased (Fig. 4g, h). This result suggested that SMART did
184 not monitor apoptosis in pMEFs.
185
186 **Administration of cisplatin induces necroptosis in renal proximal tubular cells.** We
187 tested whether *in vivo* imaging of necroptosis was feasible with SMART Tg mice.
188 Previous studies have shown that necroptosis occurred *in vivo* in murine models of
189 TNF-induced SIRS, ischemic reperfusion injuries, and cisplatin-induced kidney injuries
190 [35, 36, 37]. After considering which models and organs would be most suitable and

191 technically feasible for imaging necroptosis *in vivo* with two-photon excitation

192 microscopy, we focused on cisplatin-induced kidney injury.

193 Previous studies reported that administration of cisplatin induces renal

194 proximal tubular cell necroptosis, and this injury is attenuated in *Ripk3-/-* mice [37, 38]. We

195 found that cisplatin injections resulted in gradual increases in blood urea nitrogen

196 (BUN) and serum creatinine levels in wild-type (WT) mice (Fig. 5a). These signs were

197 accompanied by kidney damage, such as the dilatation of the proximal tubule lumens

198 (Fig. 5b). We then investigated whether phospho-RIPK3 (pRIPK3)-positive cells, a

199 hallmark of necroptosis, appeared in the kidney after cisplatin injection. We found that,

200 after the cisplatin injection, the numbers of pRIPK3-positive cells gradually increased

201 and peaked on day 2 in the renal cortex of wild-type mice (Fig. 5c, e). We also found

202 cells that cleaved caspase 3 (CC3)-positive cells appeared in the kidneys of wild-type

203 mice after the cisplatin injection (Fig. 5d, f). These findings suggested that cisplatin-

204 induced both apoptosis and necroptosis in the kidney. In contrast to the previous studies

205 [37, 38], cisplatin-induced kidney injury was not attenuated, but rather exacerbated in

206 *Ripk3*$^{-/-}$ mice compared to WT mice (Fig. 5g). Of note, pRIPK3^{+} cells were completely

207 abolished in the kidneys of *Ripk3*$^{-/-}$ mice (Fig. 5h), but the numbers of CC3^{+} cells were

208 increased in the kidneys of *Ripk3*$^{-/-}$ mice (Fig. 6i, j).

209

210 **SMART monitors necroptosis in renal proximal tubular cells after cisplatin**

211 **administration**. We then tested whether the FRET/CFP ratio was increased in SMART

212 Tg mice with cisplatin-induced kidney injuries. Given that pRIPK3-positive cells

213 peaked on day 2 after the cisplatin injection (Fig. 5c, e, h), we analyzed necroptosis by

214 *in vivo* imaging on day 2. Almost all proximal tubule lumens were patent in untreated

215 mice, and these proximal tubular cells did not show the increased FRET/CFP ratios

216 (Fig. 6a, *upper panel*). However, in cisplatin-treated mice, many proximal tubule

217 lumens were occluded, and several proximal tubules showed the increased FRET/CFP

218 ratios on day 2 (Fig. 6a, *lower panel*). To investigate the kinetics of the occlusion of

219 proximal tubule lumens and the increased FRET/CFP ratios, we visualized these two

220 events by live imaging following cisplatin injection on day 2. In untreated mice, most

221 proximal tubule lumens remained patent during the imaging periods (Supplementary

222 movie 4). In sharp contrast, a few proximal tubule lumens were patent at the start of the

223 imaging, but these tubule lumens were eventually occluded during the imaging periods

224 (Fig. 6b, Supplementary Movie 5). The FRET/CFP ratio of proximal tubular cells was

225 increased and peaked at approximately 100 min after the occlusion of the proximal

226 tubule lumens (Fig. 6b, c). These results suggested that the increase in the FRET/CFP

227 ratio may be associated with the occlusion of the tubule lumens and that SMART could

228 monitor necroptosis of the proximal tubular cells.

229 To evaluate the increase in the FRET/CFP ratios in the kidneys more

230 quantitatively, we calculated the averaged FRET/CFP ratios of each tubule in the

231 kidneys of untreated and cisplatin-treated mice, during the same periods, on day 2 after

232 the injection. We found significantly higher average FRET/CFP ratios in the kidneys of

233 cisplatin-treated mice compared to the kidneys in untreated mice (Fig. 6d, e). In

234 contrast, the averaged FRET/CFP ratios in SMART *Ripk3-/-* mice after the cisplatin

235 injection were comparable to those observed in untreated SMART *Ripk3-/-* mice (Fig.

236 6f, g). Taken together, these results indicated that SMART could monitor renal proximal

237 tubular cell necroptosis *in vivo*.

238

239 **Discussion**

240 In the present study, we generated transgenic mice that stably expressed the FRET
241 biosensor, SMART, in various tissues. Consistent with our previous study [22], we could
242 efficiently monitor necroptosis *in vitro* in primary cells isolated from SMART Tg mice,
243 such as macrophages and MEFs. Moreover, we could image cells in SMART Tg mice *in*
244 *vivo* with two-photon excitation microscopy. We found that the FRET/CFP ratio in renal
245 proximal tubular cells was elevated in cisplatin-treated mice compared to untreated
246 mice. Taken together, these findings suggested that SMART Tg mice may be a valuable
247 tool for visualizing necroptosis *in vivo*. It remains unclear whether we will be able to
248 monitor necroptosis in all cells prepared from SMART Tg mice; nevertheless, SMART
249 Tg mice may be useful for FRET analyses in various types of primary cells.

250 In contrast to apoptosis, which normally occurs in different developmental
251 stages, necroptosis does not play a major role in development. However, necroptosis is
252 involved in various pathological conditions, including TNF-mediated SIRS, ischemic
253 reperfusion injuries, virus infections, neurodegeneration, and drug-induced tissue
254 injuries [1, 2]. Therefore, we first tested whether TNF-induced SIRS in SMART Tg mice
255 might be a useful model for visualizing necroptosis *in vivo*. In contrast to several
256 previous studies, which showed that intestinal epithelial cells die by necroptosis after

257 injecting high concentrations of TNF [35, 36], we found that only small numbers of
258 intestinal epithelial cells expressed pRIPK3. Moreover, small intestine peristalsis
259 prevented live-cell imaging of necroptosis with two-photon excitation microscopy.
260 Considering organ accessibility from an external position, we decided to study
261 the cisplatin-induced kidney injury model in SMART Tg mice. IHC revealed that
262 pRIPK3^{+} cells appeared in the kidney on day 2 following cisplatin injection. This
263 relatively delayed kinetics of the appearance of necroptotic cells prevented the standard
264 *in vivo* imaging from determining the FRET/CFP ratio before and after cisplatin
265 stimulation. Therefore, we started imaging the FRET/CFP ratio of proximal tubular
266 cells in the kidneys on day 2 following cisplatin injection. Although we expected that it
267 would be difficult to capture cells undergoing necroptosis during short-term imaging (~
268 2 h), we acquired images in SMART Tg mice that showed the increased FRET/CFP
269 ratio in several renal proximal tubular cells. Of note, the increased FRET/CFP ratio in
270 tubular cells usually occurred after the occlusion of proximal tubule lumens, suggesting
271 that induction of necroptosis does not appear to be an initial event of tubular injury, but
272 rather a late event following occlusion of proximal tubule lumens. As our present study
273 did not investigate the causal relationship between the induction of the FRET and the

274 occlusion of tubule lumens, we cannot formally exclude the possibility that these two
275 events are independent, but occur simultaneously.
276 Of note, the numbers of cells showing the increased FRET/CFP ratios were
277 relatively few, even in the occluded tubules of the cisplatin-treated kidneys of SMART
278 Tg mice. This suggests that another type of cell death, such as apoptosis, ferroptosis, or
279 necrosis, may simultaneously occur in cisplatin-induced kidney injury [39, 40]. The
280 mechanisms underlying cisplatin-induced necroptosis are still a matter of debate. A
281 previous study reported that cisplatin-induced nephrotoxicity is mediated by TNF
282 produced by renal parenchymal cells [41]. In contrast, a later study reported that combined
283 treatment of renal tubular cells with TNF, TNF-like weak inducer of apoptosis
284 (TWEAK), and IFNγ, but not TNF alone, results in necroptosis [37]. Moreover, under the
285 conditions where expression of IAPs is attenuated by chemotherapeutic agents, such as
286 etoposide and doxorubicin, the cell death-inducing signaling complex, termed the
287 Ripoptosome, is spontaneously formed in the absence of death ligand stimulation [42, 43].
288 The Ripoptosome comprises RIPK1, caspase 8, and FADD, thereby inducing apoptosis
289 or necroptosis in a context-dependent manner [42, 43]. Taken together, one might surmise
290 that cisplatin treatment induces downregulation of the expression of IAPs that triggers
291 the Ripoptosome formation, further increasing the susceptibility of renal proximal

292 tubular cells to TNF- or TWEAK-induced apoptosis or necroptosis. Consistent with this
293 idea, the RIPK1 inhibitor has been shown to suppress cisplatin-induced necroptosis [44].
294 Further study will be required to investigate this possibility.

295 FRET/CFP ratio elevations in renal tubular cells were not observed in SMART
296 *Ripk3-/-* mice. That finding suggested that elevations in the FRET/CFP ratios depended
297 on RIPK3 expression. In contrast to the previous studies [37, 44], BUN and serum
298 creatinine levels and numbers of $CC3^{+}$ cells were increased in *Ripk3*$^{-/-}$ mice compared
299 to wild-type mice following cisplatin injection, at least under our experimental
300 conditions. Although the mechanisms underlying the discrepancy between our and
301 previous results are currently unknown, one can surmise that DAMPs released from
302 necroptotic tubular cells may attenuate cisplatin-induced apoptosis.

303 Necroptotic cells may release large amounts of intracellular content into the
304 extracellular space, resulting in various cellular responses [20]. Although we previously
305 succeeded in simultaneously imaging the execution of necroptosis and the release of
306 HMGB1 *in vitro* [22], it remains largely unknown where and when DAMPs are released
307 from necroptotic cells *in vivo*. To address this issue, it will be crucial to generate
308 transgenic mice that express DAMPs fused to a fluorescent protein, such as HMGB1-
309 mCherry. Then, a new mouse line could be generated by crossing SMART mice with

310 HMGB1-mCherry mice. That model might allow the visualization of DAMP release

311 and necroptosis simultaneously, at single-cell resolution. *In vivo* imaging with SMART

312 Tg mice could pave the way to a better understanding of necroptosis-induced biological

313 responses *in vivo*.

314

315 ## Methods

316 **Reagents.** We purchased the following reagents as follows: BV6 (B4653, ApexBio),
317 cisplatin (AG-CR1-3590, Adipogen), GSK'872 (530389, Merck), IFNβ (12401-1, PBL-
318 Assay Science), LPS (434, List Labs), nigericin (AG-CN2-0020, Adipogen), Murine
319 TNF (34-8321, eBioscience), zVAD (3188-v, Peptide Institute), and 5z7Ox (499610,
320 Millipore). The following antibodies were used in this study: anti-actin (A2066, Sigma-
321 Aldrich, diluted 1:1000), anti-cleaved caspase 3 (9661, Cell Signaling Technology,
322 diluted 1:1000), phycoerythrin (PE) cyanine-7–conjugated anti-CD11b (101215,
323 Biolegend, diluted 1:100), PE-conjugated anti-F4/80 (50-4801, TOMBO biosciences,
324 diluted 1:100), anti-green fluorescent protein (GFP) (sc-8334, Santa Cruz
325 Biotechnology, diluted 1:5000), anti-MLKL (3H1, Millipore, diluted 1:1000), anti-
326 phospho-RIPK3 (57220, Cell Signaling Technology, diluted 1:1000), horseradish
327 peroxidase (HRP)–conjugated donkey anti-rat IgG (712-035-153, Jackson
328 ImmunoResearch Laboratories, Inc, 1:20000), HRP–conjugated donkey anti-rabbit IgG
329 (NA934, GE Healthcare, 1:20000), biotin-conjugated donkey anti-rabbit IgG (E0432,
330 Dako, 1:200), and Streptavidin-HRP (P0397, Dako, 1:300).
331

332 **Cell culture.** Primary MEFs (pMEFs) were prepared from SMART Tg mice at E14.5
333 after coitus with a standard method. We prepared immortalized wild-type and *Mlkl*-/-
334 MEFs (iMEFs) described previously [22]. MEFs were maintained in DMEM medium
335 containing 10% fetal bovine serum (FBS).
336
337 **Mice.** *Ripk3*-/- mice[45] (provided by Genentech Inc.) were described previously.
338 C57BL/6 mice (Sankyo Lab Service) were housed in a specific pathogen-free facility
339 and received a routine chow diet and water *ad libitum*. All animal experiments were
340 performed according to the guidelines approved by the Institutional Animal
341 Experiments Committee of Toho University School of Medicine (approval number: 21-
342 54-400), Kyoto Graduate School of Medicine (approval number: Medkyo 21562), and
343 the RIKEN Kobe branch (approval number: QA2013-04-11).
344
345 **Generation of SMART Tg mice.** SMART Tg mice were generated by microinjecting
346 *Tol2* mRNA and the pT2KXIG-mSMART vector into the cytoplasm of fertilized eggs
347 from C57BL/6 mice, as described previously[26]. Eight- to twelve-week-old male and
348 female mice were used for the *in vivo* imaging.
349

350 **Western blotting.** Murine tissues were homogenized with a Polytron (Kinematica, Inc.)
351 and lysed in RIPA buffer (50 mM Tris-HCl, pH 8.0, 150 mM NaCl, 1% Nonidet P-40,
352 0.5% deoxycholate, 0.1% SDS, 25 mM β-glycerophosphate, 1 mM sodium orthovanadate,
353 1 mM sodium fluoride, 1 mM phenylmethylsulfonyl fluoride, 1 μg/ml aprotinin, 1 μg/ml
354 leupeptin, and 1 μg/ml pepstatin). After centrifugation, cell lysates were subjected to SDS
355 polyacrylamide gel electrophoresis and transferred onto polyvinylidene difluoride
356 membranes (IPVH 00010, Millipore). The membranes were immunoblotted with the
357 indicated antibodies and developed with Super Signal West Dura Extended Duration
358 Substrate (34076, Thermo Scientific). The signals were analyzed with an Amersham
359 Imager 600 (GE Healthcare Life Sciences).
360
361 **Flow cytometry.** Cells were stained with anti-CD11b and anti-F4/80 antibodies in flow
362 cytometry staining buffer (eBioscience). The prepared cells were gated on forward and
363 side scatter to identify the lymphocyte population, and then discriminating doublets.
364 Cells were analyzed with a BD FACSCant II flow cytometer (BD Biosciences) and
365 FlowJo software (BD Biosciences).
366

367 **Cell death assay.** Macrophages were plated onto 96-well plates and cultured for 12 h in
368 RPMI medium containing 10% FBS. Macrophages were stimulated with the IAP
369 antagonist, BV6 (1 μM), in the presence of the apoptosis inhibitor, zVAD (20 μM), the
370 RIPK3 inhibitor, GSK'872 (5 μM), or both, as indicated, for the times indicated. To
371 induce pyroptosis, macrophages were pretreated with LPS (1 ng/mL) for 4 h, then
372 stimulated with nigericin (10 μM) for the indicated times. Primary MEFs were
373 untreated or pretreated with IFNβ (2000 IU/mL) for 24 h, then stimulated with TNF (10
374 ng/mL) and BV6 in the presence of zVAD (20 μM) or GSK'872 (5 μM), as indicated,
375 for 18 h. The concentrations of LDH released from cells were determined with a
376 Cytotoxicity Detection Kit (Roche), as described previously [46].
377 In some experiments, macrophages were pretreated with LPS (1 ng/mL) for 4 h,
378 and then stimulated with 5z7Ox (125 nM) in the presence of zVAD (20 μM), GSK'872
379 (5 μM), or both, as indicated, for 4 h. Cell viability was determined with a water-soluble
380 tetrazolium salts assay (Cell Counting kit-8, Dojindo Molecular Technologies).
381
382 **FRET analysis *in vitro.*** FRET analysis was performed as previously described. Briefly,
383 FRET signals were imaged with a DeltaVision microscope system (GE healthcare) built
384 on an Olympus IX-71 inverted microscope base equipped with a Photometric Coolsnap

385 HQ2 CCD camera and a 60×/NA1.516 PlanApo oil immersion lens (Olympus). For
386 live-cell imaging FRET sensors, cells were seeded on gelatin-coated CELLview Cell
387 Culture Dishes (Greiner Bio-One) and maintained in an incubator at 37°C with 5% CO_2.
388 For imaging, cells were observed with a Blue excitation filter (400-454 nm), two
389 emission filters (blue-green, 463-487 nm for ECFP; yellow-green, 537-559 nm for
390 Ypet), and a C-Y-m polychronic mirror. The FRET emission ratio (FRET/CFP) was
391 calculated with SoftWoRx (Applied Precision Inc) by dividing the excitation at 436 nm
392 and emission at 560 nm (FRET) by the excitation at 436 nm and emission at 470 nm
393 (CFP). For statistical analyses, the obtained images were analyzed with ImageJ and
394 MetaMorph software. The ΔFRET/CFP ratios were calculated by subtracting the
395 FRET/CFP ratio at time 0 from the FRET/CFP ratio at the indicated times.
396
397 **Isolation of peritoneal exudate macrophages.** To isolate peritoneal exudate
398 macrophages, 6- to 8-week-old mice of the indicated genotypes were intraperitoneally
399 injected with 2.5 ml 3% thioglycollate (T9032, Sigma). On day 4 after the thioglycollate
400 injection, anesthetized mice were intraperitoneally injected with ice-cold PBS; then, the
401 peritoneal cells were harvested when the PBS was recovered. This procedure was
402 repeated twice. Harvested cells were placed in plates with RPMI medium. After

403 removing non-adherent cells, the remaining cells were primarily peritoneal

404 macrophages. Approximately 80% of these cells were positively stained with CD11b

405 and F4/80 antibodies.

406

407 **Injection of cisplatin into mice.** To produce cisplatin-induced kidney injuries, 8- to 12-

408 week-old mice of the indicated genotypes were injected with cisplatin (20 mg/kg).

409 Injected mice were sacrificed at the indicated times, and sera and kidney tissues were

410 collected for subsequent analyses.

411

412 **Histological, immunohistochemical, and immunofluorescence analyses.** Tissues were

413 fixed in 10% formalin and embedded in paraffin blocks. Paraffin-embedded kidney

414 sections were used for hematoxylin and eosin staining, immunohistochemistry, and

415 immunofluorescence analyses. For immunohistochemistry, paraffin-embedded sections

416 were treated with Instant Citrate Buffer Solution (RM-102C, LSI Medicine) for antigen

417 retrieval. Next, tissue sections were stained with anti-CC3 antibody, followed by the

418 secondary antibody, biotin-conjugated anti-rabbit antibody. Streptavidin-HRP was added

419 for visualization. Images were acquired with an all-in-one microscope (BZ-X700,

420 Keyence) and analyzed with a BZ-X Analyzer (Keyence). $CC3^{+}$ cells were automatically

421 counted in three randomly selected high-power fields (original magnification, ×40) per
422 kidney, with a Hybrid Cell Count (Keyence).
423 For the immunofluorescence analyses, tissue sections were preincubated with
424 MaxBlock™ Autofluorescence Reducing Kit (MaxVision Biosciences), according to the
425 manufacturer's instructions. Next, tissue sections were stained with anti-pRIPK3
426 antibody, followed by visualization with the tyramide signal amplification method,
427 according to the manufacturer's instructions (NEL741001KT, Kiko-tech). Images were
428 acquired with an LSM 880 (Zeiss). The images were processed and analyzed with ZEN
429 software (Zeiss) and an image-processing package, Fiji (https://fiji.sc/). pRIPK3^{+} cells
430 were counted manually.
431
432 **Measurement of blood urea nitrogen and creatinine.** After the cisplatin injection,
433 serum samples were collected on days 0, 1, 2, and 3. Serum creatinine (measured with an
434 enzymatic method) and blood urea nitrogen (measured with the urease-glutamate
435 dehydrogenase method) were measured by Oriental Yeast.
436
437 **Imaging cisplatin-induced kidney injury.** Living mice were observed with an
438 FV1200MPE-BX61WI upright microscope (Olympus) equipped with an XLPLN 25XW-

439 MP 25X/1.05 water-immersion objective lens (Olympus). The microscope was equipped
440 with an InSight DeepSee Ultrafast laser (0.95 Watt, 900 nm; Spectra-Physics, Mountain
441 View, CA). The scan speed was set at 2 μs/pixel. The excitation wavelength for CFP was
442 840 nm. Fluorescence images were acquired with the following filters and mirrors: an
443 infrared-cut filter (BA685RIF-3); two dichroic mirrors (DM505 and DM570); and three
444 emission filters, including: an FF01-425/30 (Semrock, Rochester, NY), for the second
445 harmonic generation; a BA460-500 (Olympus) for CFP; and a BA520-560 (Olympus) for
446 FRET. The microscope was also equipped with a two-channel GaAsP detector unit and
447 two multi-alkali detectors. FluoView software (Olympus) was used to control the
448 microscope and acquire images. Acquired images were saved in the multilayer 12-bit
449 tagged image file format and processed and analyzed with Metamorph software, as
450 described previously [47].

451 Intravital mouse imaging was performed essentially as described previously [47].
452 Briefly, two days before imaging, cisplatin was injected intravenously. To observe the
453 kidney, the mouse was placed in the prone position on an electric heat pad maintained at
454 37°C. A 1-cm incision was made in the skin of the lower back and underlying peritoneum
455 to expose approximately 0.25 cm^2 of tissue. The exposed tissue was imaged with an
456 aspiration fixation system. The obtained images were analyzed by Metamorph. The

457 FRET/CFP ratios of relevant areas were calculated with ImageJ software. Then, the
458 averaged FRET/CFP ratios were calculated for each proximal tubule.
459
460 **Statistical analysis.** Statistical analyses were performed with the unpaired two-tailed
461 Student's *t*-test or one-way or two-way ANOVA with Dunnett's, Sidak's, or Tukey's
462 multiple comparison test, as appropriate. *P*-values <0.05 were considered statistically
463 significant.
464
465

466 **Acknowledgments**

467 We thank K. Asano for technical advice, Genentech Inc. for *Ripk3*-/- mice, M.
468 Pasparakis for *Mlkl*-/- MEFs, and K. Kawakami for the transposon-based expression
469 vector system. This work was supported, in part, by Grants-in-Aid for Scientific
470 Research (B) 20H03475 (to HN), Scientific Research (C) 19K07399 (to KM), and
471 Scientific Research (C) 20K05238 (to SM) from the Japan Society for the Promotion of
472 Science (JSPS), a Grant-in-Aid for Scientific Research on Innovative Areas
473 (JP16H06280) — Platforms for Advanced Technologies and Research Resources
474 "Advanced Bioimaging Support", from the Japan Agency for Medical Research and
475 Development (AMED), under Grant Numbers 21gm1210002 (to HN) and
476 21wm0325050 (to KM), grants from the Ministry of Education, Culture, Sports,
477 Science, and Technology, Japan, Toho University Grant for Research Initiative Program
478 (TUGRIP) (to HN), the Science Research Promotion Fund, and The Promotion and
479 Mutual Aid Corporation for Private Schools of Japan (to HN), a GSK Japan Research
480 Grant 2020 (to KM), and a grant from the Takeda Science Foundation (to KM).

481

482 **Author Contributions**

483 S.M., K.M., Kenta T., M.M., and H.N. designed research; S.M., Kanako T., and S.K.-S.

484 performed research; K.S., K.A., and M.O. contributed to new reagents/analytical tools;

485 S.M., Kanako T., K.M., Kenta T., Y.Y., T.M., M. M., and H.N. analyzed data; S.M. and

486 H.N. wrote the manuscript.

487

488 **Conflict of Interest**

489 The authors declare no conflict of interest.

490

491 **Biological materials availability**

492 All the biological materials, including SMART Tg mice used in this study, are available

493 from the corresponding authors upon reasonable request. Obtaining *Ripk3*-/- mice

494 requires Material Transfer Agreement (MTA) from Genentech Inc.

495

496 **Data availability**

497 The authors declare that the data supporting this study are available within the paper and

498 its supplementary movies. Source data behind the graphs are available as source data files.

499 Other datasets generated during and/or analyzed during the current study are available

500 from the corresponding author upon reasonable request.

References

1. Zhou W, Yuan J. Necroptosis in health and diseases. *Semin Cell Dev Biol* **35**, 14-23 (2014).

2. Tonnus W, Linkermann A. The in vivo evidence for regulated necrosis. *Immunol Rev* **277**, 128-149 (2017).

3. Weinlich R, Oberst A, Beere HM, Green DR. Necroptosis in development, inflammation and disease. *Nat Rev Mol Cell Biol* **18**, 127-136 (2017).

4. Chan FK, Luz NF, Moriwaki K. Programmed necrosis in the cross talk of cell death and inflammation. *Annu Rev Immunol* **33**, 79-106 (2015).

5. Grootjans S, Vanden Berghe T, Vandenabeele P. Initiation and execution mechanisms of necroptosis: an overview. *Cell Death Differ* **24**, 1184-1195 (2017).

6. Annibaldi A, Walczak H. Death Receptors and Their Ligands in Inflammatory Disease and Cancer. *Cold Spring Harb Perspect Biol* **12**, (2020).

7. Micheau O, Tschopp J. Induction of TNF receptor I-mediated apoptosis via two sequential signaling complexes. *Cell* **114**, 181-190 (2003).

8. Newton K*, et al.* Cleavage of RIPK1 by caspase-8 is crucial for limiting apoptosis and necroptosis. *Nature* **574**, 428-431 (2019).

9. Zhang X, Dowling JP, Zhang J. RIPK1 can mediate apoptosis in addition to necroptosis during embryonic development. *Cell Death Dis* **10**, 245 (2019).

10. Cho YS*, et al.* Phosphorylation-driven assembly of the RIP1-RIP3 complex regulates programmed necrosis and virus-induced inflammation. *Cell* **137**, 1112-1123 (2009).

11. He S*, et al.* Receptor interacting protein kinase-3 determines cellular necrotic response to TNF-alpha. *Cell* **137**, 1100-1111 (2009).

536 12. Moriwaki K, Chan FK. RIP3: a molecular switch for necrosis and inflammation.
537 *Genes Dev* **27**, 1640-1649 (2013).
538
539 13. Mompean M*, et al.* The Structure of the Necrosome RIPK1-RIPK3 Core, a
540 Human Hetero-Amyloid Signaling Complex. *Cell* **173**, 1244-1253 e1210 (2018).
541
542 14. Li J*, et al.* The RIP1/RIP3 necrosome forms a functional amyloid signaling
543 complex required for programmed necrosis. *Cell* **150**, 339-350 (2012).
544
545 15. Sun L*, et al.* Mixed lineage kinase domain-like protein mediates necrosis
546 signaling downstream of RIP3 kinase. *Cell* **148**, 213-227 (2012).
547
548 16. Cai Z*, et al.* Plasma membrane translocation of trimerized MLKL protein is
549 required for TNF-induced necroptosis. *Nat Cell Biol* **16**, 55-65 (2014).
550
551 17. Dondelinger Y*, et al.* MLKL compromises plasma membrane integrity by binding
552 to phosphatidylinositol phosphates. *Cell Rep* **7**, 971-981 (2014).
553
554 18. Wang H*, et al.* Mixed lineage kinase domain-like protein MLKL causes necrotic
555 membrane disruption upon phosphorylation by RIP3. *Mol Cell* **54**, 133-146
556 (2014).
557
558 19. Chen X*, et al.* Translocation of mixed lineage kinase domain-like protein to
559 plasma membrane leads to necrotic cell death. *Cell Res* **24**, 105-121 (2014).
560
561 20. Nakano H, Murai S, Moriwaki K. Regulation of the release of damage-associated
562 molecular patterns from necroptotic cells. *Biochem J* **479**, 677-685 (2022).
563
564 21. Kaczmarek A, Vandenabeele P, Krysko DV. Necroptosis: the release of damage-
565 associated molecular patterns and its physiological relevance. *Immunity* **38**, 209-
566 223 (2013).
567
568 22. Murai S*, et al.* A FRET biosensor for necroptosis uncovers two different modes
569 of the release of DAMPs. *Nat Commun* **9**, 4457 (2018).
570
571 23. Shirasaki Y*, et al.* Real-time single-cell imaging of protein secretion. *Sci Rep* **4**,

572 4736 (2014).
573
574 24. Yamagishi M, Shirasaki Y. Live-Cell Imaging Technique to Visualize DAMPs
575 Release During Regulated Cell Death. *Methods Mol Biol* **2274**, 337-352 (2021).
576
577 25. Nakano H, Murai S, Yamaguchi Y, Shirasaki Y, Nakabayashi O, Yamazaki S.
578 Development of novel methods that monitor necroptosis and the release of
579 DAMPs at the single cell resolution. *Cell Stress* **3**, 66-69 (2019).
580
581 26. Sumiyama K, Kawakami K, Yagita K. A simple and highly efficient transgenesis
582 method in mice with the Tol2 transposon system and cytoplasmic microinjection.
583 *Genomics* **95**, 306-311 (2010).
584
585 27. Vince JE*, et al.* IAP antagonists target cIAP1 to induce TNFalpha-dependent
586 apoptosis. *Cell* **131**, 682-693 (2007).
587
588 28. Varfolomeev E*, et al.* IAP antagonists induce autoubiquitination of c-IAPs, NF-
589 kappaB activation, and TNFalpha-dependent apoptosis. *Cell* **131**, 669-681 (2007).
590
591 29. Orning P*, et al.* Pathogen blockade of TAK1 triggers caspase-8-dependent
592 cleavage of gasdermin D and cell death. *Science* **362**, 1064-1069 (2018).
593
594 30. Varga Z*, et al.* Differences in the sensitivity of classically and alternatively
595 activated macrophages to TAK1 inhibitor-induced necroptosis. *Cancer Immunol*
596 *Immunother* **69**, 2193-2207 (2020).
597
598 31. Wang JS, Wu D, Huang DY, Lin WW. TAK1 inhibition-induced RIP1-dependent
599 apoptosis in murine macrophages relies on constitutive TNF-alpha signaling and
600 ROS production. *J Biomed Sci* **22**, 76 (2015).
601
602 32. Pasparakis M, Vandenabeele P. Necroptosis and its role in inflammation. *Nature*
603 **517**, 311-320 (2015).
604
605 33. Sarhan J*, et al.* Constitutive interferon signaling maintains critical threshold of
606 MLKL expression to license necroptosis. *Cell Death Differ* **26**, 332-347 (2019).
607

608 34. Knuth AK, Rosler S, Schenk B, Kowald L, van Wijk SJL, Fulda S. Interferons
609 Transcriptionally Up-Regulate MLKL Expression in Cancer Cells. *Neoplasia* **21**,
610 74-81 (2019).
611
612 35. Newton K*, et al.* RIPK3 deficiency or catalytically inactive RIPK1 provides
613 greater benefit than MLKL deficiency in mouse models of inflammation and
614 tissue injury. *Cell Death Differ* **23**, 1565-1576 (2016).
615
616 36. Duprez L*, et al.* RIP kinase-dependent necrosis drives lethal systemic
617 inflammatory response syndrome. *Immunity* **35**, 908-918 (2011).
618
619 37. Xu Y*, et al.* A Role for Tubular Necroptosis in Cisplatin-Induced AKI. *J Am Soc*
620 *Nephrol* **26**, 2647-2658 (2015).
621
622 38. Wang JN*, et al.* RIPK1 inhibitor Cpd-71 attenuates renal dysfunction in cisplatin-
623 treated mice via attenuating necroptosis, inflammation and oxidative stress. *Clin*
624 *Sci (Lond)* **133**, 1609-1627 (2019).
625
626 39. McSweeney KR, Gadanec LK, Qaradakhi T, Ali BA, Zulli A, Apostolopoulos V.
627 Mechanisms of Cisplatin-Induced Acute Kidney Injury: Pathological
628 Mechanisms, Pharmacological Interventions, and Genetic Mitigations. *Cancers*
629 *(Basel)* **13**, (2021).
630
631 40. Hu J, Gu W, Ma N, Fan X, Ci X. Leonurine alleviates ferroptosis in cisplatin-
632 induced acute kidney injury by activating the Nrf2 signalling pathway. *Br J*
633 *Pharmacol*, (2022).
634
635 41. Zhang B, Ramesh G, Norbury CC, Reeves WB. Cisplatin-induced nephrotoxicity
636 is mediated by tumor necrosis factor-alpha produced by renal parenchymal cells.
637 *Kidney Int* **72**, 37-44 (2007).
638
639 42. Tenev T*, et al.* The Ripoptosome, a signaling platform that assembles in response
640 to genotoxic stress and loss of IAPs. *Mol Cell* **43**, 432-448 (2011).
641
642 43. Feoktistova M*, et al.* cIAPs block Ripoptosome formation, a RIP1/caspase-8
643 containing intracellular cell death complex differentially regulated by cFLIP

644 isoforms. *Mol Cell* **43**, 449-463 (2011).
645
646 44. Meng XM*, et al.* Wogonin protects against cisplatin-induced acute kidney injury
647 by targeting RIPK1-mediated necroptosis. *Lab Invest* **98**, 79-94 (2018).
648
649 45. Newton K, Sun X, Dixit VM. Kinase RIP3 is dispensable for normal NF-kappa
650 Bs, signaling by the B-cell and T-cell receptors, tumor necrosis factor receptor 1,
651 and Toll-like receptors 2 and 4. *Mol Cell Biol* **24**, 1464-1469 (2004).
652
653 46. Piao X*, et al.* Depletion of myeloid cells exacerbates hepatitis and induces an
654 aberrant increase in histone H3 in mouse serum. *Hepatology* **65**, 237-252 (2017).
655
656 47. Kamioka Y*, et al.* Live imaging of protein kinase activities in transgenic mice
657 expressing FRET biosensors. *Cell Struct Funct* **37**, 65-73 (2012).
658
659
660

661 **Figure legends**

662 **Figure 1. Generation of SMART Tg mice. a,** Depiction of the SMART biosensor
663 structure (*top*) and its activation mechanism (*bottom*). Ypet, modified yellow fluorescent
664 protein; ECFP, enhanced cyan fluorescent protein; pRIPK3, phosphorylated RIPK3. **b,**
665 Western blots probed with anti-GFP antibody show expression of the SMART biosensor
666 in various murine tissues. Tissue extracts were prepared from the indicated organs of 8-
667 week-old wild-type or SMART Tg mice. Results are representative of two independent
668 experiments. **c**, Mice were intraperitoneally injected with thioglycollate, then peritoneal
669 cells were recovered by washing the peritoneal cavity with ice-cold PBS on day 4 after
670 injection. Isolated cells were stained with the indicated antibodies and analyzed with flow
671 cytometry. The percentages of $CD11b^{+}F4/80^{+}$ cells indicate the fraction of macrophages;
672 the levels of YFP detected in these cell populations indicate the expression of SMART.
673 Results are representative of three independent experiments. WT, wild-type. **d**, Peritoneal
674 macrophages from SMART Tg mice were untreated or stimulated with BV6 (1 μM) +
675 zVAD (20 μM) or BV6 (1 μM) + zVAD (20 μM) + GSK'872 (5 μM) for the indicated
676 times. Cell death was assessed with the LDH release assay. Results are mean ± SD of
677 triplicate samples, and they are representative of five independent experiments. **e, f,**
678 Peritoneal macrophages derived from SMART Tg mice were stimulated as described in

679 **d**, and FRET/CFP ratios were calculated. Pseudocolored images show cellular changes in
680 FRET/CFP ratio values in response to the indicated stimulations (**e**). FRET/CFP
681 responses are color-coded according to the color scales (*right*). White arrowheads indicate
682 cells undergoing necroptosis. Scale bars, 20 μm. Maximum changes detected in the
683 FRET/CFP ratios (**f**). Results are mean ± SE (n = 11 cells per condition). Each dot
684 indicates an individual cell. Results are representative of four independent experiments.
685 Statistical significance was determined with two-way ANOVA with Dunnett's multiple
686 comparison test (**d**) or one-way ANOVA with Turkey's multiple comparison test (**f**).
687 ****P<0.0001; ns, not significant.
688
689 **Figure 2. SMART does not monitor pyroptosis or apoptosis**. **a**, Peritoneal
690 macrophages isolated from SMART mice were pretreated with LPS (1 ng/mL) for 4 h,
691 then stimulated with nigericin (10 μM) for the indicated times. Cell death was determined
692 with the LDH release assay. Results are mean ± SD of triplicate samples and
693 representative of three independent experiments. **b, c**, Peritoneal macrophages were
694 stimulated as described in **a**, and the FRET/CFP ratio was calculated. Pseudocolored
695 images show cellular changes in FRET/CFP ratio values in response to the indicated
696 stimulations (**b**). FRET/CFP responses are color-coded according to the color scales

697 (*right*). White arrows indicate cells undergoing pyroptosis. Scale bars, 20 μm. Maximum
698 changes detected in the FRET/CFP ratios (**c**). Results are mean ± SE (n = 8 cells per
699 condition). Each dot indicates an individual cell. Results are representative of three
700 independent experiments. Statistical analysis was performed with the unpaired two-tailed
701 Student's *t*-test. ns, not significant. **d**, Peritoneal macrophages from SMART Tg mice
702 were pretreated with LPS (1 ng/mL) for 4 h, then stimulated with the indicated
703 combination of agents (125 nM 5z7Ox, 5 μM GSK'872, 20 μM zVAD) for 4 h. Cell
704 viability was determined with the WST assay. Results are mean ± SD of triplicate samples.
705 Representative results of four independent experiments. **e, f,** Peritoneal macrophages
706 were stimulated as described in **d**. Macrophages are displayed as pseudocolor images to
707 show cellular changes in FRET/CFP ratio values in response to the indicated stimulations
708 (**e**). FRET/CFP responses are color-coded according to the color scales (*right*). White
709 arrowheads indicate cells undergoing necroptosis. Scale bars, 20 μm. Maximum changes
710 detected in the FRET/CFP ratios of the cells (**f**). Results are mean ± SE (n = 10 cells per
711 condition). Each dot indicates an individual cell. Results are representative of two
712 independent experiments. Statistical significance was determined with two-way ANOVA
713 with Sidak's multiple comparison test (**a**), the unpaired two-tailed Student *t*-test (**c**), or
714 one-way ANOVA with Tukey's multiple comparison analysis (**d, f**). ****P<0.0001; ns,

715 not significant.

716

717 **Figure 3. SMART monitors necroptosis in a RIPK3-dependent manner**. **a**,

718 Peritoneal macrophages from SMART WT or SMART *Ripk3*$^{-/-}$ mice were untreated or

719 stimulated with BV6 (1 μM) + zVAD (20 μM) or BV6 (1 μM) + zVAD (20 μM) +

720 GSK'872 (5 μM) for the indicated periods. Cell death was determined with the LDH

721 release assay. Results are mean ± SD of triplicate samples. **b, c**, Peritoneal macrophages

722 were stimulated and analyzed as described in **a**. Pseudocolored images show cellular

723 changes in FRET/CFP ratio values in response to the indicated stimulations (**b**).

724 FRET/CFP responses are color-coded according to the color scales (*right*). White

725 arrowheads indicate cells undergoing necroptosis. Scale bars, 20 μm. Maximum

726 changes detected in the FRET/CFP ratio (**c**). Results are mean ± SE (n = 10 cells). Each

727 dot indicates an individual cell. Statistical analysis was performed with two-way

728 ANOVA with Tukey's multiple comparisons test (**a**, *left panel*) or Sidak's multiple

729 comparison test (**a**, *right panel*), one-way ANOVA with Tukey's multiple comparison

730 test (**c**, *left panel*), or the unpaired two-tailed Student *t*-test (**c**, *right panel*). ****P

731 <0.0001; ns, not significant. All results are representative of three independent

732 experiments.

733

734 **Figure 4. SMART monitors necroptosis, but not apoptosis, in MEFs. a, b**, primary

735 MEFs (pMEFs) (**a**) and immortalized MEFs (iMEFs) (**b**) were untreated or stimulated

736 with TBZ (10 ng/mL TNF, 1 μM BV6, 20 μM zVAD) for 12 h. MEFs were generated

737 from SMART Tg mice, and MEFs with less than five passages were used as pMEFs.

738 Cell death was determined with the LDH release assay. Results are mean ± SD of

739 triplicate samples. **c**, Western blots of lysates from untreated iMEFs from *Mlkl*-/- or

740 wild-type mice, and untreated or IFNβ (2,000 IU/mL)-treated pMEFs from SMART Tg

741 mice. Blots were probed with anti-MLKL and anti-actin antibodies. **d**, pMEFs were

742 pretreated with IFNβ, and then stimulated with TBZ. Cell viability was determined with

743 the LDH release assay. Results are mean ± SD of triplicate samples. **e-h**, pMEFs were

744 untreated or stimulated with the indicated combination of agents (10 ng/mL TNF, 1 μM

745 BV6, 20 μM zVAD, 5 μM GSK'872), and the FRET/CFP ratios were calculated.

746 Pseudocolored images show cellular changes in the FRET/CFP ratio values in response

747 to the indicated stimulations (**e, g**). FRET/CFP responses are color-coded according to

748 the color scales (*right*). White arrowheads and white arrows indicate cells undergoing

749 necroptosis (**e**) and apoptosis (**g**), respectively. Scale bars, 20 μm. Maximum changes

750 were detected in the FRET/CFP ratios (**f, h**). Results mean ± SE (n = 10 cells per

751 condition). Each dot indicates an individual cell. Statistical analyses were performed by

752 the unpaired two-tailed Student's *t*-test (**a, b, d, h**) or one-way ANOVA with Tukey's

753 multiple comparison test (**f**). ***P<0.001; ****P<0.0001; ns, not significant. All results

754 are representative of at least two independent experiments.

755

756 **Figure 5. Administration of cisplatin induces necroptosis in renal proximal tubular**

757 **cells. a-f,** Eight-week-old wild-type were intravenously injected with cisplatin (20

758 mg/kg), then sacrificed at the indicated times. Concentrations of blood urea nitrogen

759 (BUN) and serum creatinine were determined at the indicated times after cisplatin

760 treatment (**a**). Results are mean ± SE (n = 3 mice per time point). Results are

761 representative of two independent experiments. Kidney tissue sections were prepared at

762 the indicated times after cisplatin treatment and stained with hematoxylin & eosin (n = 5

763 mice) (**b**). Scale bar, 50 μm. Asterisks indicate dilated proximal tubules. Kidney tissue

764 sections were stained with anti-phospho-RIPK3 (pRIPK3) (**c**) or anti-cleaved caspase 3

765 (CC3) (**d**) antibodies. White arrowheads and black arrows indicate pRIPK3^{+} and CC3^{+}

766 cells, respectively. Scale bars, 50 μm. Cell counts for pRIPK3^{+} (**e**) and CC3^{+} (**f**) cells,

767 expressed as the number of positive cells per field. Results are mean ± SE (n = 5 mice).

768 **g-j**, Eight-week-old wild-type and *Ripk3*$^{-/-}$ mice were injected with cisplatin as in **a** and

769 sacrificed on day 2 after injection (wild-type, n = 5 mice; *Ripk3*$^{-/-}$ mice, n = 6 mice).

770 Concentrations of BUN and serum creatinine were determined as in **a** (**g**). Kidney tissue

771 sections were stained with anti-pRIPK3 (**h**) or anti-CC3 (**i**) antibodies. Scale bars, 50

772 μm. The numbers of CC3^{+} cells were counted as in **f** (**j**). White arrowheads and black

773 arrows indicate pRIPK3^{+} and CC3^{+} cells, respectively. Statistical analyses were

774 performed with one-way ANOVA and Dunnett's multiple comparison test (**a, e, f**) or the

775 unpaired two-tailed Student t-test (**g, j**). ***P<0.001; ns, not significant.

776

777 **Figure 6. SMART monitors necroptosis in renal proximal tubular cells after**

778 **cisplatin administration. a-c,** Eight- to twelve-week-old SMART Tg mice were

779 untreated or treated with 20 mg/kg cisplatin. On day 2, the left-side kidneys of untreated

780 and cisplatin-treated mice were analyzed with two-photon excitation microscopy.

781 Black-and-white and pseudocolored images show CFP intensities and the FRET/CFP

782 ratios, respectively, in kidneys of untreated (*upper panel*) or cisplatin-treated (*lower*

783 *panel*) wild-type mice (**a**). FRET/CFP responses are color-coded according to the color

784 scales. Scale bars, 50 μm. Magnified images of the areas in **a** outlined in white boxes

785 (**b**). Dotted white lines indicate proximal tubule lumens. White arrowheads indicate

786 cells that show increases in the FRET/CFP ratios. FRET/CFP responses are color-coded

787 according to the color scales. Scale bars, 50 μm. Graphs show CFP intensities (*blue*)

788 and the FRET/CFP ratios (*pink*) of the cells indicated in **b**, calculated at the times

789 indicated (**c**). Red arrows indicate the time that the tubule lumens were occluded. **d-g**,

790 Eight- to twelve-week-old SMART WT mice (**d**) or SMART *Ripk3*-/- mice (**f**) were

791 untreated or treated with cisplatin, as described in **a**. FRET/CFP responses are color-

792 coded according to the color scales. Scale bars, 50 μm. Graphs show the averaged

793 FRET/CFP ratios observed in tubules from untreated or cisplatin-treated SMART WT

794 (**e**) or SMART *Ripk3*-/- (**g**) mice. Results are mean ± SE (n = 70 tubules in SMART WT

795 mice; n = 40 tubules in SMART *Ripk3*$^{-/-}$ mice). Each number indicates an individual

796 mouse. Results are representative of two independent experiments. Statistical analyses

797 were performed by one-way ANOVA with Dunnett's multiple comparison test.

798 ****P<0.0001; ns, not significant.

799

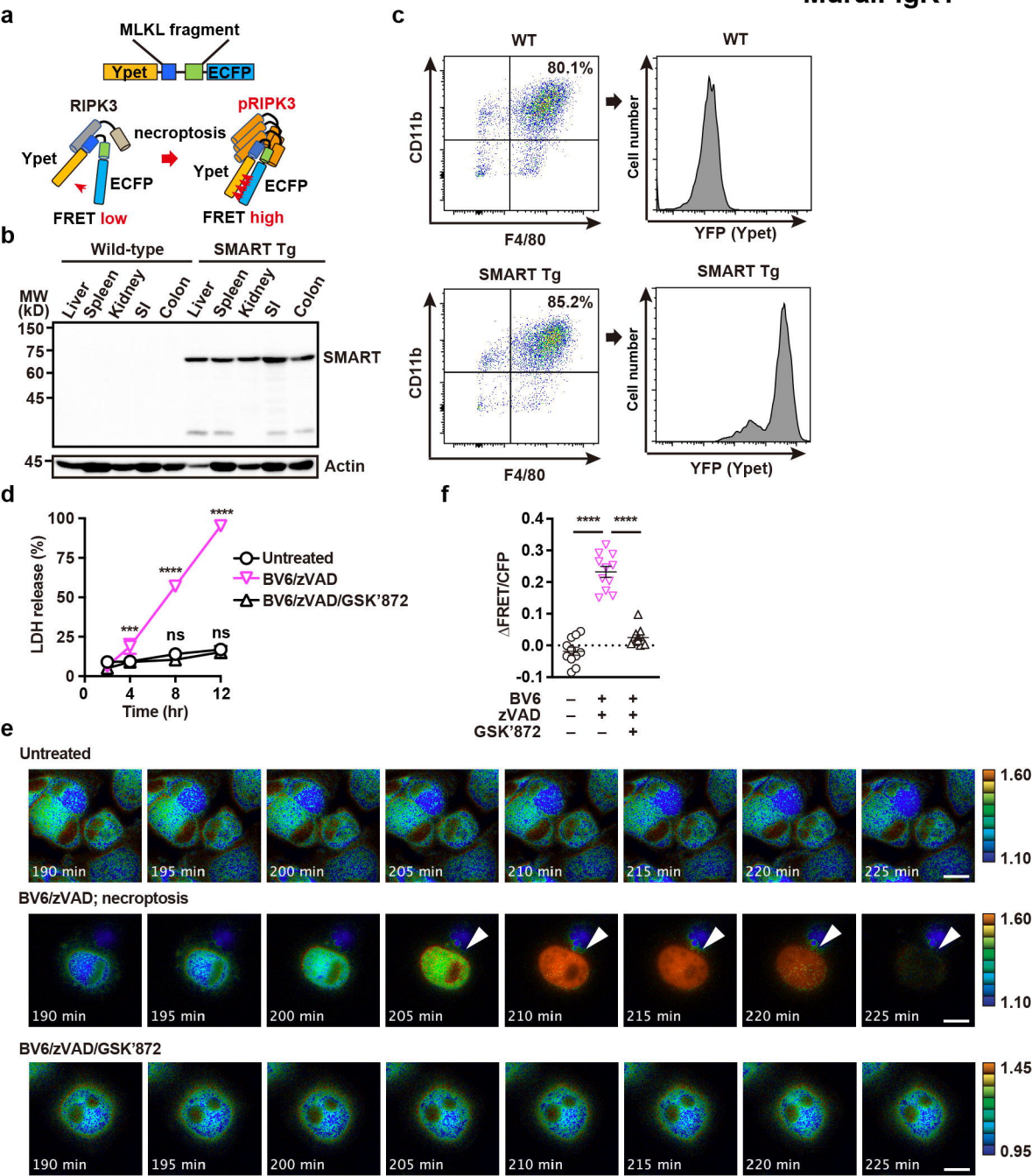
a
MLKL fragment
Ypet
ECFP
RIPK3
pRIPK3
necroptosis
Ypet
ECFP
FRET low
FRET high
b
Wild-type
SMART Tg
MW (kD)
Liver
Spleen
Kidney
SI
Colon
150
75
60
45
SMART
Actin
c
WT
80.1%
CD11b
F4/80
Cell number
YFP (Ypet)
SMART Tg
85.2%
d
LDH release (%)
Time (hr)
Untreated
BV6/zVAD
BV6/zVAD/GSK'872
***
****
ns
e
Untreated
BV6/zVAD; necroptosis
BV6/zVAD/GSK'872
190 min
195 min
200 min
205 min
210 min
215 min
220 min
225 min
1.60
1.10
1.45
0.95
f
ΔFRET/CFP
BV6
zVAD
GSK'872

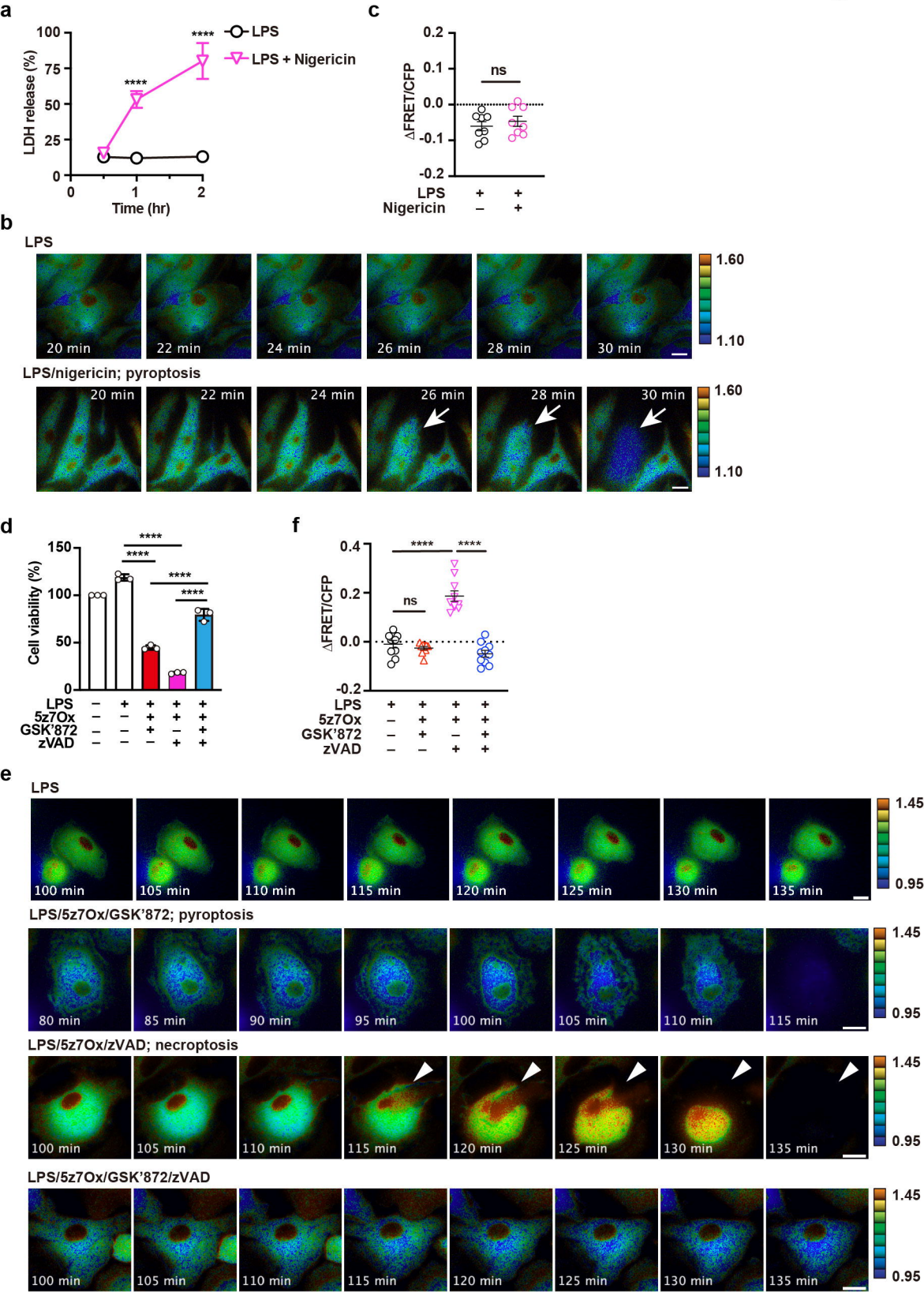
a
LDH release (%)
Time (hr)
LPS
LPS + Nigericin
****
c
ΔFRET/CFP
ns
LPS
Nigericin
b
LPS
20 min
22 min
24 min
26 min
28 min
30 min
1.60
1.10
LPS/nigericin; pyroptosis
d
Cell viability (%)
LPS
5z7Ox
GSK'872
zVAD
f
e
LPS
100 min
105 min
110 min
115 min
120 min
125 min
130 min
135 min
1.45
0.95
LPS/5z7Ox/GSK'872; pyroptosis
80 min
85 min
90 min
95 min
LPS/5z7Ox/zVAD; necroptosis
LPS/5z7Ox/GSK'872/zVAD

MuraiFigR3

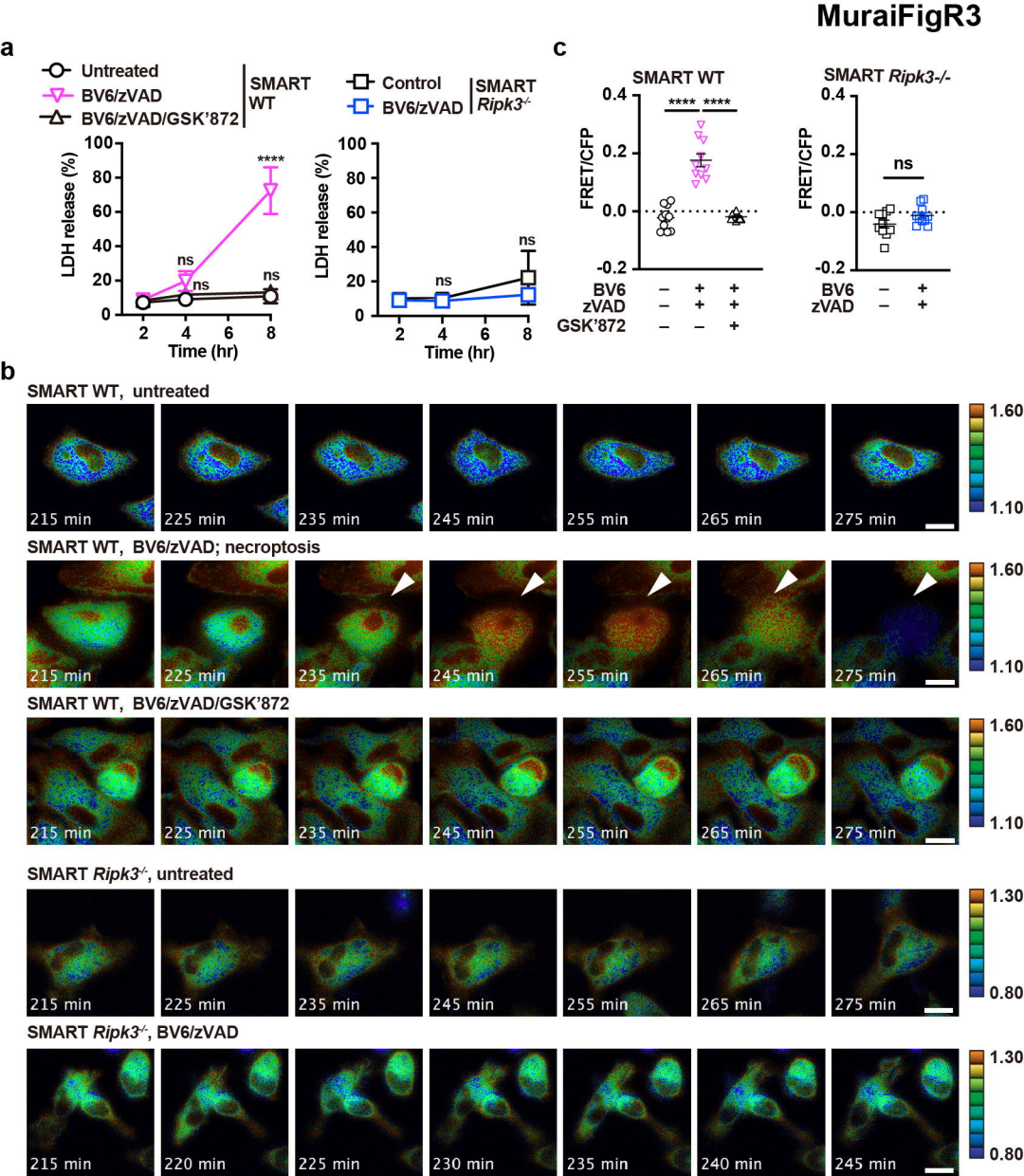
a
Untreated
BV6/zVAD
BV6/zVAD/GSK'872
SMART WT
LDH release (%)
Time (hr)
****
ns
Control
BV6/zVAD
SMART Ripk3-/-
c
SMART WT
SMART Ripk3-/-
FRET/CFP
BV6
zVAD
GSK'872
b
SMART WT, untreated
SMART WT, BV6/zVAD; necroptosis
SMART WT, BV6/zVAD/GSK'872
SMART Ripk3-/-, untreated
SMART Ripk3-/-, BV6/zVAD
215 min
220 min
225 min
230 min
235 min
240 min
245 min
255 min
265 min
275 min
1.60
1.10
1.30
0.80

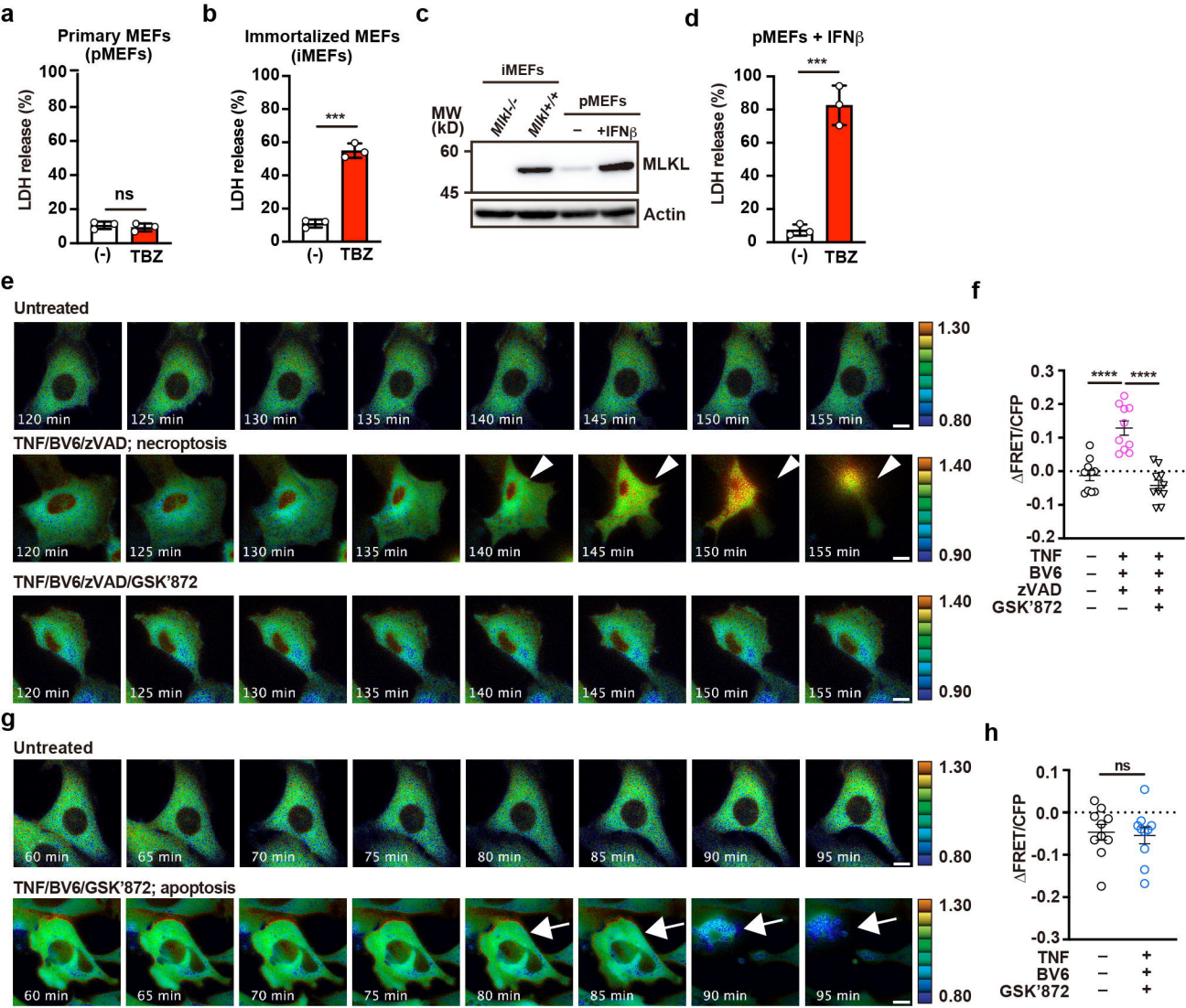
a
Primary MEFs (pMEFs)
LDH release (%)
ns
(-)
TBZ
b
Immortalized MEFs (iMEFs)
LDH release (%)
***
(-)
TBZ
c
iMEFs
pMEFs
MW (kD)
Mlkl-/-
Mlkl+/+
–
+IFNβ
60
45
MLKL
Actin
d
pMEFs + IFNβ
LDH release (%)
***
(-)
TBZ
e
Untreated
TNF/BV6/zVAD; necroptosis
TNF/BV6/zVAD/GSK'872
120 min
125 min
130 min
135 min
140 min
145 min
150 min
155 min
1.30
0.80
1.40
0.90
f
ΔFRET/CFP
****
****
TNF
BV6
zVAD
GSK'872
g
Untreated
TNF/BV6/GSK'872; apoptosis
60 min
65 min
70 min
75 min
80 min
85 min
90 min
95 min
1.30
0.80
h
ΔFRET/CFP
ns
TNF
BV6
GSK'872

MuraiFigR5

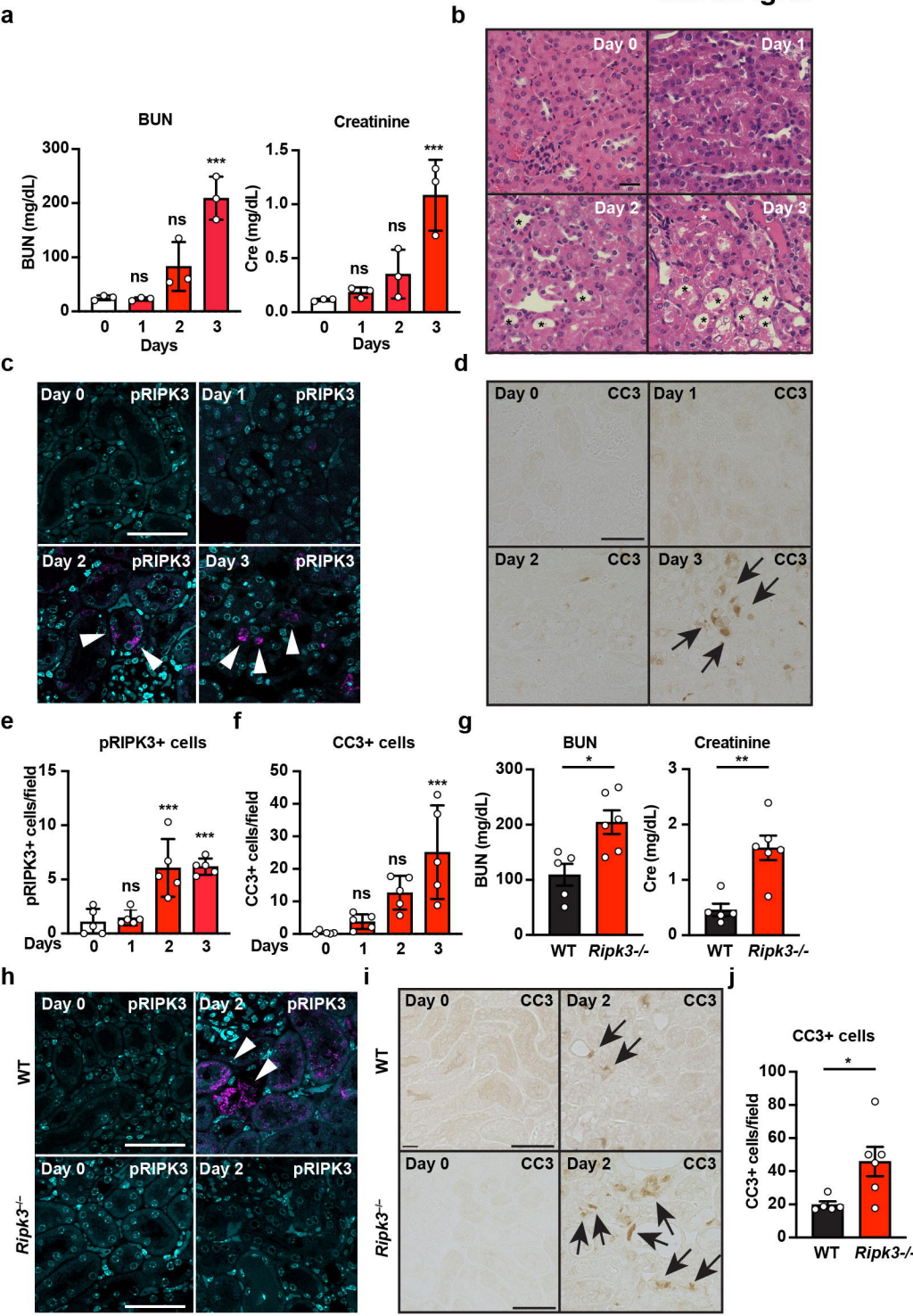
a
BUN
Creatinine
BUN (mg/dL)
Cre (mg/dL)
Days
ns
***
b
Day 0
Day 1
Day 2
Day 3
c
pRIPK3
d
CC3
e
pRIPK3+ cells
pRIPK3+ cells/field
f
CC3+ cells
CC3+ cells/field
g
BUN
Creatinine
WT
Ripk3-/-
h
i
j
CC3+ cells

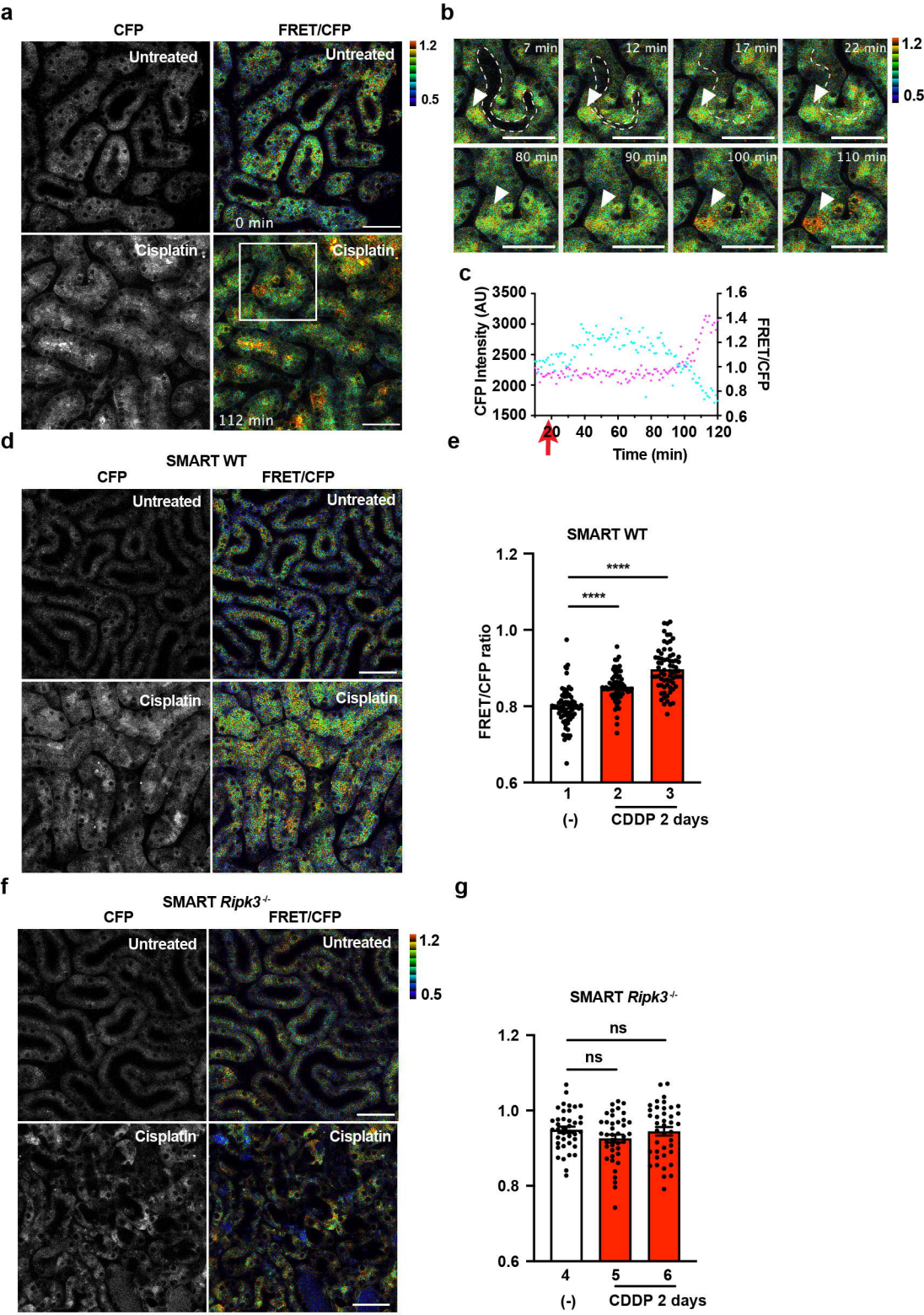
a
CFP
FRET/CFP
Untreated
Untreated
0 min
Cisplatin
Cisplatin
112 min
1.2
0.5
b
7 min
12 min
17 min
22 min
80 min
90 min
100 min
110 min
1.2
0.5
c
CFP Intensity (AU)
FRET/CFP
Time (min)
d
SMART WT
CFP
FRET/CFP
Untreated
Untreated
Cisplatin
Cisplatin
e
SMART WT
FRET/CFP ratio
****
****
(-)
CDDP 2 days
f
SMART Ripk3-/-
CFP
FRET/CFP
Untreated
Untreated
Cisplatin
Cisplatin
1.2
0.5
g
SMART Ripk3-/-
ns
ns
(-)
CDDP 2 days